Design and Performance Analysis of Quadruple Gate InAlN/GaN MOS-High Electron Mobility Transistor

S. K. Hima Bindhu, Yogesh Kumar Verma and Kamal Bhatia

ABSTRACT

The short-channel effects in single-gate (SG) field-effect transistors are significant due to poor control of the gate on the channel. Accordingly, in this work, we have designed a quadruple-gate (QG) AlInN/GaN MOS-HEMT and performed a comparative analysis of both SG and QG structures. The comparison of the different electrical parameters is performed for different temperature and doping concentration. It is analyzed that doping concentration significantly affects the electrical performance and the magnitude of electrical parameters significantly varies with variations in temperature and doping concentration. It is noticed that the cut-off frequency is comparatively higher for QG structure, thus highlighting it as a potential contender for different RF applications.

Keywords: Quadruple gate, Single gate, AlInN, GaN, MOS-HEMT

School of Electronics and Electrical Engineering, Lovely Professional University, Jalandhar, India ROR

Correspondence to:
Yogesh Kumar Verma,
yogesh.25263@lpu.co.in

Additional material is published online only. To view please visit the journal online.

Cite this as: Hima Bindhu SK, Verma YK and Bhatia K. Design and Performance Analysis of Quadruple Gate InAlN/GaN MOS-High Electron Mobility Transistor. Premier Journal of Science 2025;15:100248

DOI: https://doi.org/10.70389/PJS.100248

Peer Review

Received: 22 August 2025

Last revised: 31 October 2025

Accepted: 17 December 2025

Version accepted: 4

Published: 31 January 2026

Ethical approval: N/a

Consent: N/a

Funding: No industry funding

Conflicts of interest: N/a

Author contribution:
S. K. Hima Bindhu, Yogesh Kumar Verma and Kamal Bhatia – Conceptualization, Writing – original draft, review and editing

Introduction

The electrical performance of HEMT depends on different device parameters such as temperature, channel height, thickness of oxide layer, and length of the channel. The analysis of HEMT is performed by several research groups to analyze its electrical performance using different techniques.[1–3] Huque et al.[4] proposed an analytical model for AlGaN/GaN power HEMT to calculate the DC performance at higher temperatures. Turuvekere et al.[5] analyzed the gate-leakage mechanisms of AlInN/GaN and AlGaN/GaN HEMTs considering thermionic emission (TE), Poole-Frenkel emission (PF), and Fowler Nordheim tunneling (FN). TE and PF mechanisms are dominant in AlGaN/GaN and FN is dominant in AlInN/GaN HEMT and predicted that Schottky barrier height increases with temperature. The temperature significantly effects the transconductance of both quadruple-gate (QG) and single-gate (SG) due to phonon scattering and mobility variation. The phonon scattering represents the interactions between the charge carriers and vibrations of the crystal lattice, which are quantized as phonons.[6–10] It is noticed that the transconductance is higher for low values of temperatures at higher values of gate voltage. He et al.[11] calculated the DC and AC characteristics of Al-N/β-Ga_2O_3 HEMT, and reported that the drain current is reduced with increase in temperature that leads to the decrease in the transconductance. At lower temperature, the phonon scattering is reduced and carrier mobility increases significantly. At higher temperature, lower carrier mobility and increased interface trap activity is there. At higher gate voltage, stronger channel control and higher 2-DEG density is obtained due to which the cut-off frequency is reduced. In this work, the output conductance, transconductance generation factor, and early voltage of multi- gate and single gate AlInN/GaN MOS HEMT are compared. It is noticed that the QG AlInN/GaN MOS HEMT exhibits lower output conductance (g_d) as compared to single gate (SG) so QG can operate at higher currents with less variation. The effect of variation in temperature is also analyzed on different electrical parameters.

Structure of the Device

Figure 1 represents the 3D structure of AlInN/GaN MOS HEMT. The AlInN barrier layer provides lattice matching with GaN thus reduces the strain and damage at the hetero-interface thus improving the stability of the structure. The usage of oxide layer provides interesting significant features such as reducing gate leakage current and improving the breakdown voltage of the device. The GaN layer provides the confinement of the charge carriers and consists of the channel between source and drain.[6,7] The GaN layer belongs to wide bandgap material thus provides higher breakdown voltage and more voltage can be applied at the drain terminal.

Development of Model

In the present work, the analytical modeling of QG AlInN/GaN MOS-HEMT is performed. The method of equivalent number of gates is used. The parabolic potential expression is represented using Eqution (3). Tables 1 and 2 represent the device parameters and relations used in the present work. The boundary conditions are represented using Equations (4)–(9). The QG high electron mobility transistor (HEMT) can be viewed as two separate double gate (DG) HEMTs in zx and yz planes. So, we can analyze QG using the equivalent number of gates (ENG) method. The characteristics length λ_{QG} of QG can be calculated using:

$$\frac{1}{\lambda_{QG}^2}=\frac{1}{\lambda_{DGzx}^2}+\frac{1}{\lambda_{DGyz}^2} \quad (1)$$

where λ_{DGzx} and λ_{DGyz} are the characteristics length of the DG HEMTs in *zx* and *yz* planes.

Considering the DG HEMT of *zx* plane the characteristics length is calculated solving following 2D Poisson's equation:

$$\frac{\partial^2\phi(Z,x)}{\partial x^2}+\frac{\partial^2\phi(Z,x)}{\partial z^2}=\frac{-qN_d}{\varepsilon_{GaN}} \quad (2)$$

Where N_d is the donor concentration; ϕ (*x*, *z*) is the potential in the channel; ε_{Gan} is the permittivity of GaN; *q* is the unit charge in coulombs. Assuming the parabolic potential approximation in the *x* direction,

$$\phi(z,x) = c_0(z)+c_1(z)x+c_2(z)x^2 \quad (3)$$

$c_0(z)$, $c_1(z)x$, $c_2(z)$ are constants to be determined by using the following boundary conditions:

$$(0,z) = \phi_s(z) \quad (4)$$

Guarantor: Yogesh Kumar Verma

Provenance and peer-review: Unsolicited and externally peer-reviewed

Data availability statement: N/a

$$\phi\left(W_{GaN}, z\right) = \phi_s(z) \quad (5)$$

$$\phi\left(0.5W_{GaN}, z\right) = \phi_s(z) \quad (6)$$

$$\left.\frac{\partial\phi(z,x)}{\partial x}\right|_{x=0} = \frac{C_{ox}\left(\phi_S(z) - V_{GS} - V_{FB}\right)}{\varepsilon_{GaN}} \quad (7)$$

$$\left.\frac{\partial\phi(z,x)}{\partial x}\right|_{x=W_{GaN}} = -\frac{C_{ox}\left(\phi_S(z) - V_{GS} - V_{FB}\right)}{\varepsilon_{GaN}} \quad (8)$$

$$\left.\frac{\partial\phi(z,x)}{\partial x}\right|_{x=\frac{W_{GaN}}{2}} = 0 \quad (9)$$

where $C_{ox} = \frac{\varepsilon_{ox}}{t_{ox}}$ and $V_{FB} = \phi_M - \phi_{GaN}$ which is flat band voltage using Equation (4) which states that at $x = 0$ the potential is equal to the surface potential, gives

$$c_0(z) = \phi_S(z) \quad (10)$$

using Equation (7) which states at $x = 0$ the electric field can be written as

$$\frac{\partial\phi(0,z)}{\partial z} = \frac{C_{ox}}{\varepsilon_{GaN}}\left(\phi_S(z) - V_{GS} + V_{FB}\right)$$

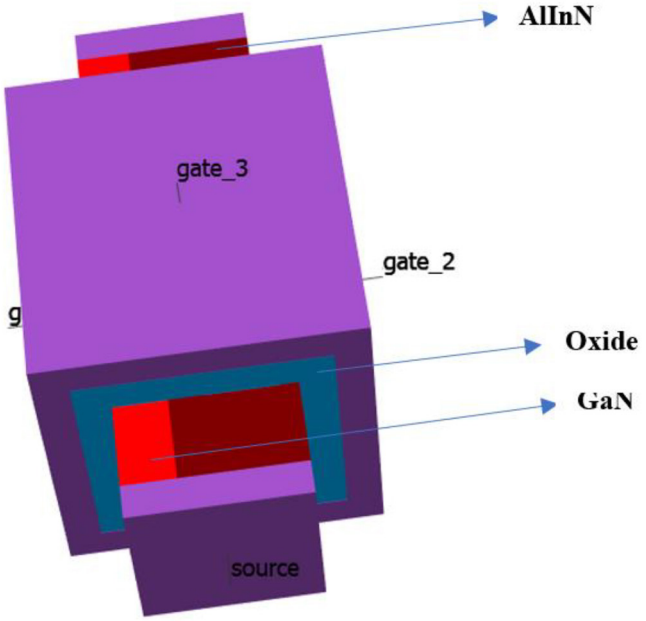

Fig 1 | 3D structure of quadruple gate AlInN/GaN MOS HEMT

Table 1 | Device Parameters	
Parameter	**Value**
t_{ox} (nm)	2
CL (nm)	20
Temperature (K)	300
H (nm)	10

gives

$$c_1(z) = \frac{C_{ox}}{\varepsilon_{GaN}}\left(\phi_S(z) - V_{GS} + V_{FB}\right) \quad (11)$$

using Equation (8) which states that at $x = W_{GaN}$ the electric field can be written as

$$\frac{\partial\phi(W_{GaN},z)}{\partial z} = -\frac{C_{ox}}{\varepsilon_{GaN}}\left(\phi_S(z) - V_{GS} + V_{FB}\right)$$

gives

$$c_2(z) = -\frac{C_{ox}\left(\phi_S(z) - V_{GS} + V_{FB}\right)}{\varepsilon_{GaN} W_{GaN}} \quad (12)$$

$c_0(z)$, $c_1(z)x$, $c_2(z)$ are substituted in the Equation (3) and from this the centre potential can be calculated by putting $x = \frac{W_{GaN}}{2}$, gives

$$\frac{\partial^2(\phi_c(z))}{\partial z^2} - \frac{8C_{ox}}{W_x\left(4\varepsilon_{GaN} + W_{GaN}C_{ox}\right)}\phi_S(z) = -\frac{qN_d}{\varepsilon_{GaN}} - \frac{8C_{ox}\left(V_{GS} - V_{FB}\right)}{W_x\left(4\varepsilon_{GaN} + W_{GaN}C_{ox}\right)} \quad (13)$$

From Equation (13) the characteristic length of zx plane DG is $\lambda_{DGxz} = \sqrt{\frac{8C_{ox}}{W_{GaN}\left(4\varepsilon_{GaN} + W_{GaN}C_{ox}\right)}}$ and similarly characteristic length of yz plane DG can be calculated to be $\lambda_{DGyz} = \sqrt{\frac{8C_{ox}}{H_{GaN}\left(4\varepsilon_{GaN} + W_{GaN}C_{ox}\right)}}$

From Equation (1) we can calculate the λ_{QG} and the solution of Equation (2) is of the form

$$\phi_c(z) = Ae^{\lambda_{QG}z} + Be^{-\lambda_{QG}z} - \frac{\beta_{QG}}{\lambda_{QG}^2}$$

where $\beta_{QG} = \lambda_{QG}^2\left(V_{GS} - V_{FB}\right) - \frac{qN_d}{\varepsilon_{GaN}}$. Constants A and B can be calculated using the boundary conditions:

Potential at source terminal is V_s

$$\phi_c(0) = V_s \quad (14a)$$

Potential at drain terminal is V_D

$$\phi_c(L) = V_D \quad (14b)$$

Table 2 | Relations Used	
VIP_2,	$VIP_2 \times \left(g_{m1} / g_{m2}\right)$
VIP_3	$VIP_2 = \sqrt{\left(24 g_{m1} / g_{m3}\right)}$
IMD_3	$IMD_3 = \left[4.5 \times \left(VIP_3\right)^3 \times g_{m3}\right]^2 \times R_s$
IIP_3	$IIP_3 = \left(2 \times g_{m1}\right) / \left(3 \times g_{m3} \times R_s\right)$
g_{m1}	$g_{m1} = \left[\partial I_{DS} / \partial V_{GS}\right]$
g_{m2}	$g_{m2} = \left(1/2!\right)\left[\partial^2 I_{DS} / \partial V_{GS}^2\right]$
g_{m3}	$g_{m3} = \left(1/3!\right)\left[\partial^3 I_{DS} / \partial V_{GS}^3\right]$

DOI: https://doi.org/10.70389/PJS.100248 | Premier Journal of Science 2025;15:100248

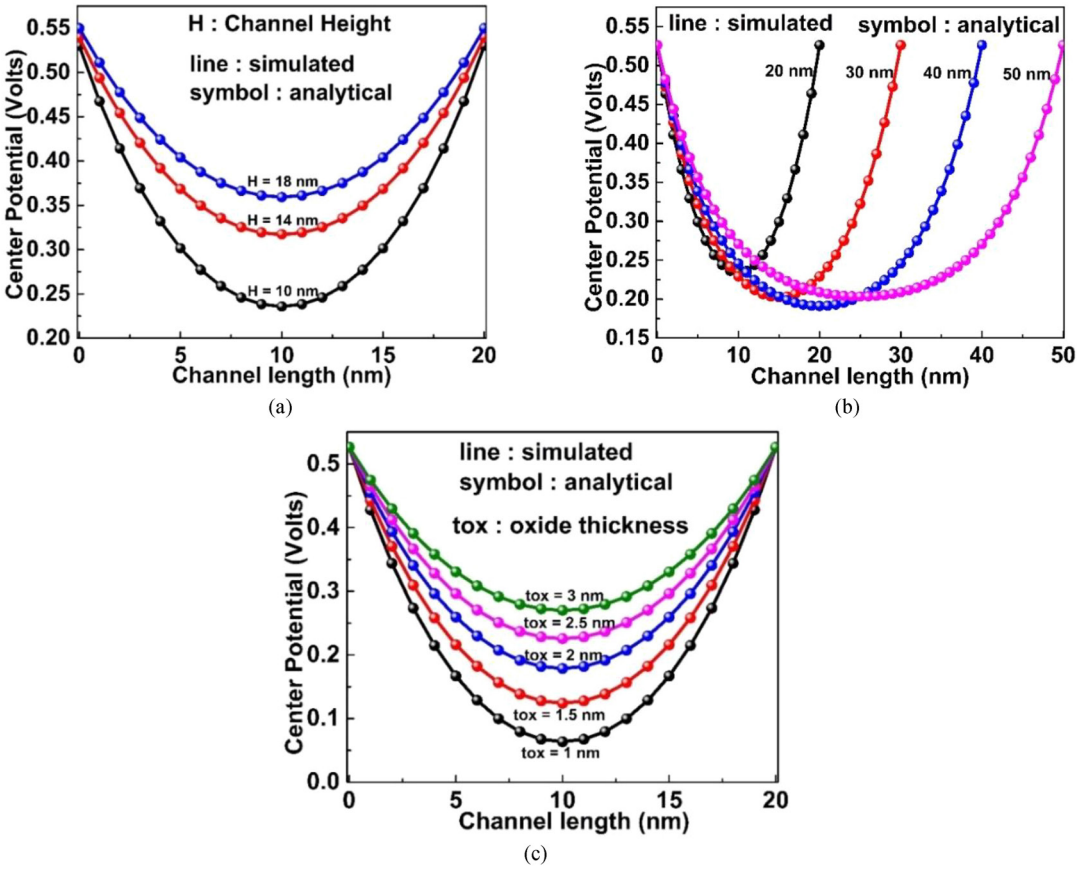

Fig 2 | Calculation of center potential for different (a) channel height (b) channel length (c) oxide thickness

Using Boundary conditions of (14a) and (14b) we get, constants A and B:

$$A=\frac{\left(V_D+\frac{\beta_{QG}}{\lambda_{QG}^2}\right)-\left(V_S+\frac{\beta_{QG}}{\lambda_{QG}^2}\right)e^{-\lambda_{QG}L}}{e^{-\lambda_{QG}L}\left(e^{2\lambda_{QG}L}-1\right)}$$
$$B=\frac{\left(V_D+\frac{\beta_{QG}}{\lambda_{QG}^2}\right)-\left(V_S+\frac{\beta_{QG}}{\lambda_{QG}^2}\right)e^{\lambda_{QG}L}}{e^{\lambda_{QG}L}\left(e^{-2\lambda_{QG}L}-1\right)} \quad (15)$$

Model Validation

The results obtained using the proposed analytical model for center potential are compared with TCAD simulations. The Albrecht model is chosen to model the low field mobility using albrct parameter. The field-dependent mobility model (FLDMOB) is used to model velocity-saturation effect. The Shockley-Read-Hall (SRH) model is initiated in the model using the SRH parameter. The concentration dependent mobility (CONMOB) model is used to account for the mobility dependent on the concentration. In order to account for the strain due to lattice mismatch CALC.STRAIN model is incorporated so that the piezoelectric-polarization effects are also included in the analysis by setting the STRAIN and POLARIZATION parameters. Figures 2a–c represent the calculation of center potential for different channel height, channel length, and oxide thickness respectively.

Results and Discussions

It is analyzed that the transconductance (g_{m1}) of both QG and SG AlInN/GaN MOS HEMT reduces with increasing temperature due to the reduction in electron mobility and increase in the gate leakage current, similar to.[9] The electron mobility reduces with the increase in temperature due increased lattice vibrations and hence increased phonon scattering. The transconductance of a semiconductor device quantifies how effectively the gate voltage controls the drain current. It is evident from Figure 3a that the magnitude of g_{m1} is higher for QG as compared to SG due to better electrostatic control and enhanced carrier modulation. The electrostatic control is improved for QG as compared to SG because the gate surrounds the channel from all the surroundings. In SG, the gate modulates only the carriers near the top of the channel; however, for QG, the gate controls the channel over the entire distribution of electrons from all the surroundings. The calculation of the first and second order derivative of transconductance,

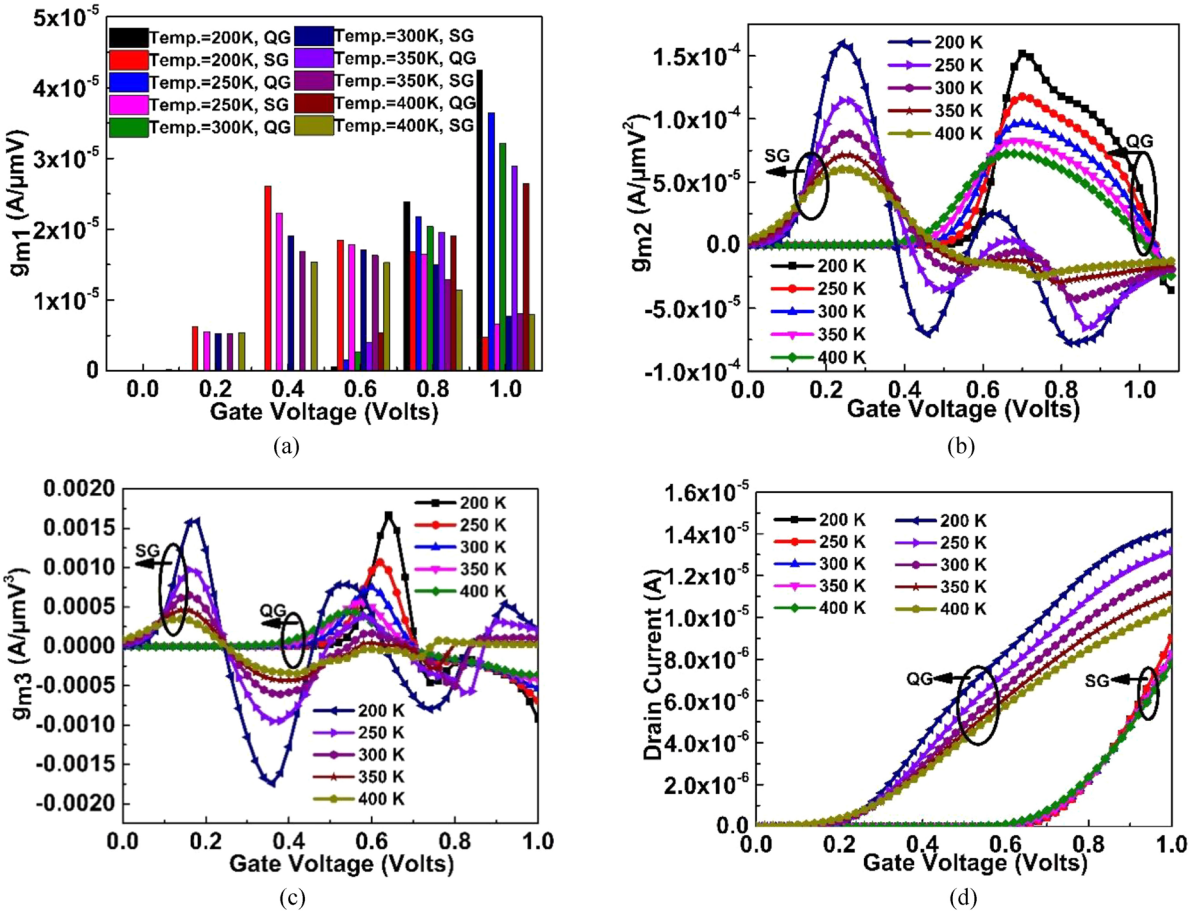

Fig 3 | Calculation of different electrical parameters w.r.t. temperature (a) g_{m1} (b) g_{m2} (c) g_{m3} (d) drain current

i.e., g_{m2} and g_{m3} for different values of temperature are represented using Figures 3b and c. The g_{m2} and g_{m3} represent that how rapidly the magnitudes of g_{m1} and g_{m2} respectively changes with V_g. It is noticed that the magnitude of g_{m2} and g_{m3} remains more stable for QG thus indicating better linearity as compared to SG. It is observed using Figure 3d that the drain current is higher at lower values of temperature due to increased mobility of electrons and reduced access and contact resistances. The phenomenon of phonon scattering is reduced at lower temperature that results in the reduced interaction of phonons with the electrons, and because of this there occurs significant reduction in the lattice vibration, resulting in the increased mobility of the electrons.

The change in doping concentration significantly affects the electrical performance of AlInN/GaN MOSHFET due to change in the charge concentration and ionized impurity scattering. Figure 4a represents the calculation of g_{m1} for different doping concentration. It is analyzed that the QG device exhibits higher magnitude of g_{m1} for different doping concentration as compared to SG, because the mobility degradation is more effective in SG at higher doping concentration. It is analyzed that the magnitude of g_{m1} is higher at higher doping concentration due to increased charge density. Figure 4b represents the comparison of cut-off frequency (f_T) for different doping concentration. It is noticed that the magnitude of f_T is higher for higher doping concentration because the magnitude of g_{m1} is increased due to increased carrier density at higher doping concentration, which leads to increase in f_T. Figure 4c represents the calculation of g_{m2} for different doping concentration. The QG device is noticed to exhibit lower magnitude of g_{m2} for different doping concentration as compared to SG due to uniform potential distribution which leads to minimal distortion. Figure 4d represents the TFP for different doping concentration. Figure 4e represents the calculation of g_{m3} for different channel length. The QG device is noticed to exhibit lower magnitude of g_{m3} for different doping concentration as compared to SG as the QG structure wraps the channel from all surroundings providing symmetric field control. Figure 4f represents the calculation of intrinsic gain. The magnitude of intrinsic gain is more in QG as compared to SG. The inversion charge is reduced more at lower doping concentration in SG than QG, thereby reducing g_{m1}, and consequently intrinsic gain is reduced more effectively as compared to QG. Figure 4g represents the comparison of IIP_3. It is noticed that QG exhibits higher IIP_3 because of the reduced magnitude of g_{m3} and increased magnitude of g_{m1} in QG as compared to SG with better electrostatic control. Figure 4h represents the comparison of VIP_2.

DOI: https://doi.org/10.70389/PJS.100248 | Premier Journal of Science 2025;15:100248

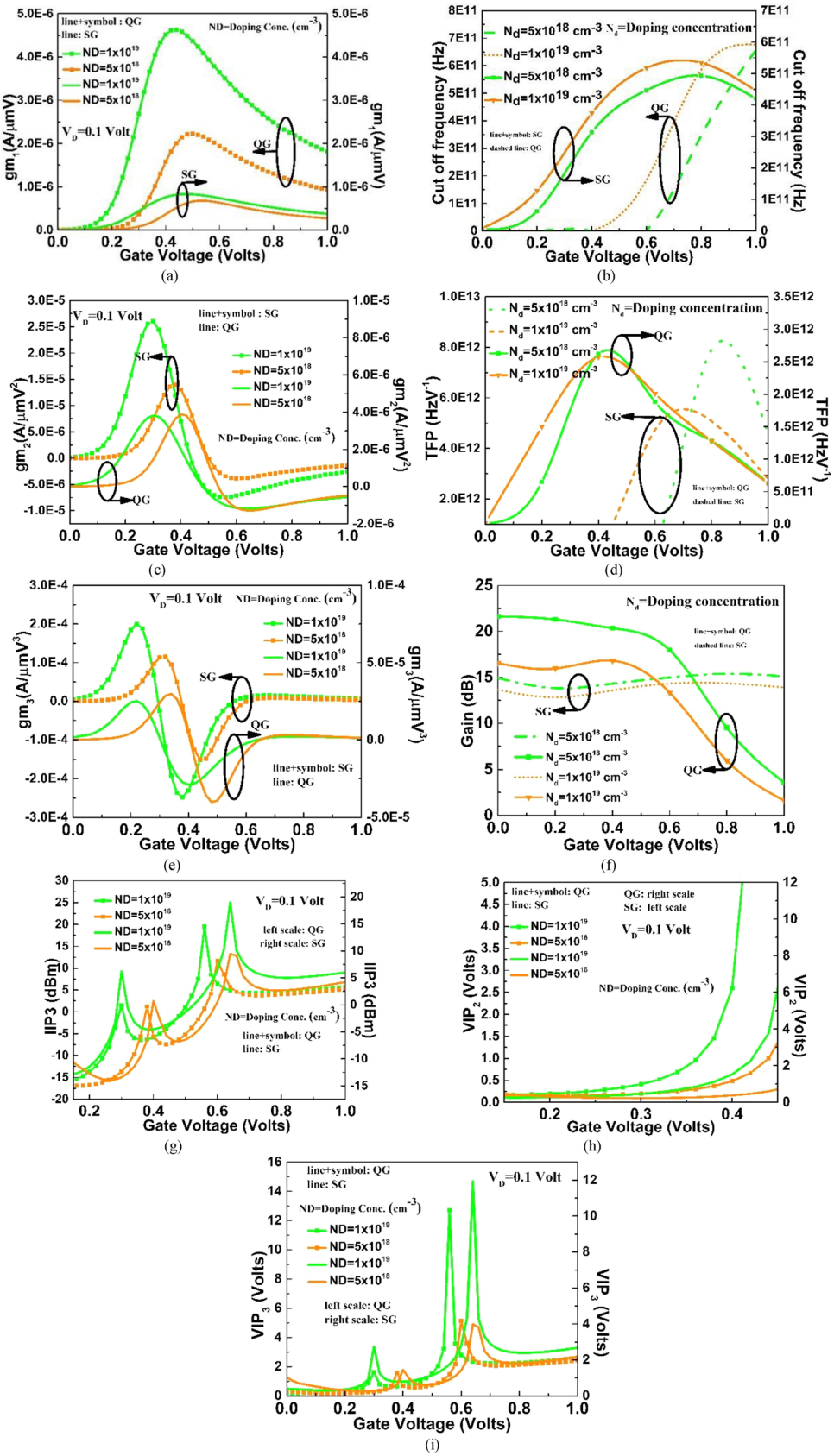

Fig 4 | Comparison of performance parameters for different doping concentration

Figure 4i represents the comparison of VIP_3. It is evident that the QG device exhibits more VIP_2 and VIP_3 as compared to SG.

Conclusion

In this work, the electrical performances of QG and SG AlInN/GaN MOS HEMTs are analyzed and compared. It

is noticed that the magnitude of g_{m2} is lower for QG as compared to SG because of better electrostatic control as channel is surrounded by the gate more effectively. The magnitude of g_{m3} is calculated lower for QG as compared to SG, highlighting reduced non-linearity. It is analyzed that the QG exhibits higher intrinsic gain as compared to SG due to increased transconductance and reduced output conductance. It is noticed that QG exhibits higher IIP_3 for the analyzed device geometry because of the reduced magnitude of g_{m3} and increased magnitude of g_{m1} in QG as compared to SG making it suitable for highly linear analog applications.

References

1 Kumar S, Soman R, Pratiyush AS, Muralidharan R, Nath DN. A performance comparison between β-Ga_2O_3 and GaN HEMTs. IEEE Trans Electron Devices. 2019;66(8):3310–7. https://doi.org/10.1109/TED.2019.2924453

2 Mishra UK, Parikh P, Wu Y-F. AlGaN/GaN HEMTs-an overview of device operation and applications. Proc IEEE. 2002;90(6):1022–31. https://doi.org/10.1109/JPROC.2002.1021567

3 Sharma N, Mishra S, Singh K, Chaturvedi N, Chauhan A, Periasamy C. High-resolution AlGaN/GaN HEMT-based electrochemical sensor for biomedical applications. IEEE Trans Electron Devices. 2019;67(1):289–95. https://doi.org/10.1109/TED.2019.2949821

4 Huque MA, Eliza SA, Rahman T, Huq HF, Islam SK. Temperature dependent analytical model for current–voltage characteristics of AlGaN/GaN power HEMT. Solid State Electron. 2009;53(3):341–8. https://doi.org/10.1109/STI53101.2021.9732585

5 Turuvekere S, Karumuri N, Rahman AA, Bhattacharya A, DasGupta A, DasGupta N. Gate leakage mechanisms in AlGaN/GaN and AlInN/GaN HEMTs: comparison and modeling. IEEE Trans Electron Devices. 2013;60(10):3157–65. https://doi.org/10.1109/TED.2013.2272700

6 Khandelwal S, Fjeldly TA. Analysis of drain-current nonlinearity using surface-potential-based model in GaAs pHEMTs. IEEE Trans Microw Theory Tech. 2013;61(9):3265–70. https://doi.org/10.1109/TMTT.2013.2275943

7 Khandelwal S, Fjeldly TA. A physics based compact model of I-V and C-V characteristics in AlGaN/GaN HEMT devices. Solid State Electron. 2012;76(March):60–66. https://doi.org/10.1016/j.sse.2012.05.054

8 Singh R, Khan MA, Mukherjee S, Kranti A. Analytical model for 2DEG density in graded MgZnO/ZnO heterostructures with cap layer. IEEE Trans Electron Devices. 2017;64(9):3661–7. https://doi.org/10.1109/TED.2017.2721437

9 Pérez-Tomás A, Fontserè A, Placidi M, Baron N, Chenot S, Moreno JC, et al. Temperature impact and analytical modeling of the AlGaN/GaN-on-Si saturation drain current and transconductance. Semicond Sci Technol. 2012;27(12):125010. https://doi.org/10.1088/0268-1242/27/12/125010

10 Turuvekere S, DasGupta A, DasGupta N. Effect of barrier layer thickness on gate leakage current in AlGaN/GaN HEMTs. IEEE Trans Electron Devices. 2015;62(10):3449–52. https://doi.org/10.1109/TED.2015.2469151

11 He X, Zhang H, Wu L, Hu J, Lu M, Yuan L. Simulation study on temperature characteristics of AlN/β-Ga2O3 HEMT. Microelectron J. 2024;152:106386. https://doi.org/10.1016/j.mejo.2024.106386